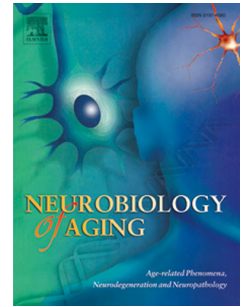


Accepted Manuscript

Human anterolateral entorhinal cortex volumes are associated with cognitive decline in aging prior to clinical diagnosis

R.K. Olsen, PhD, L.-K. Yeung, MA, A. Noly-Gandon, MSc, M.C. D'Angelo, PhD, A. Kacollja, BSc (Hons), V.M. Smith, BSc, J.D. Ryan, PhD, M.D. Barense, PhD



PII: S0197-4580(17)30153-7

DOI: [10.1016/j.neurobiolaging.2017.04.025](https://doi.org/10.1016/j.neurobiolaging.2017.04.025)

Reference: NBA 9920

To appear in: *Neurobiology of Aging*

Received Date: 12 September 2016

Revised Date: 26 April 2017

Accepted Date: 28 April 2017

Please cite this article as: Olsen, R., Yeung, L.-K, Noly-Gandon, A, D'Angelo, M., Kacollja, A, Smith, V., Ryan, J., Barense, M., Human anterolateral entorhinal cortex volumes are associated with cognitive decline in aging prior to clinical diagnosis, *Neurobiology of Aging* (2017), doi: 10.1016/j.neurobiolaging.2017.04.025.

This is a PDF file of an unedited manuscript that has been accepted for publication. As a service to our customers we are providing this early version of the manuscript. The manuscript will undergo copyediting, typesetting, and review of the resulting proof before it is published in its final form. Please note that during the production process errors may be discovered which could affect the content, and all legal disclaimers that apply to the journal pertain.

Human anterolateral entorhinal cortex volumes are associated with cognitive decline in aging prior to clinical diagnosis

RK Olsen, PhD* ^{1,2}

L-K Yeung, MA* ^{2^}

A Noly-Gandon, MSc ¹

MC D'Angelo, PhD ¹

A Kacollja, BSc (Hons) ¹

VM Smith, BSc ²

JD Ryan, PhD ^{1,2,3}

MD Barense, PhD ^{1,2}

*equal contribution

Affiliations

1 Rotman Research Institute, Baycrest Health Sciences, Toronto, ON

2 Department of Psychology, University of Toronto, Toronto, ON

3 Department of Psychiatry, University of Toronto, Toronto, ON

^ Current address:

Taub Institute

Columbia University Medical Center

630 West 168th Street

P&S Box 16

New York, NY 10032

Corresponding authors' information:

Rosanna K. Olsen

3560 Bathurst Street

Toronto, ON M6A 2E1

416-785-2500 ext 3509

rolsen@research.baycrest.org

Lok-Kin Yeung

630 West 168th Street

New York, NY 10032

212-305-2046

ly2143@cumc.columbia.edu

29 pages, 5,030 words, 2 tables, 4 figures

Abstract

We investigated whether older adults without subjective memory complaints, but who present with cognitive decline in the laboratory, demonstrate atrophy in medial temporal lobe (MTL) subregions associated with Alzheimer's disease. Forty community-dwelling older adults were categorized based on Montreal Cognitive Assessment (MoCA) performance. Total grey/white matter, cerebrospinal fluid, and white matter hyperintensity load were quantified from whole-brain T1-weighted and FLAIR magnetic resonance imaging scans, while hippocampal subfields and MTL cortical subregion volumes (CA1, dentate gyrus/CA2/3, subiculum, anterolateral and posteromedial entorhinal, perirhinal, and parahippocampal cortices) were quantified using high-resolution T2-weighted scans. Cognitive status was evaluated using standard neuropsychological assessments. No significant differences were found in the whole-brain measures. However, MTL volumetry revealed that anterolateral entorhinal cortex (alERC) volume -- the same region in which Alzheimer's pathology originates -- was strongly associated with MoCA performance. This is the first study to demonstrate that alERC volume is related to cognitive decline in undiagnosed community-dwelling older adults.

Keywords: memory, aging, hippocampus, dementia, Mild Cognitive Impairment, neuroimaging

1 Introduction

Alzheimer's disease (AD) is a devastating neurodegenerative illness with widespread societal and economic consequences. Due to the progressive nature of the disease, early and effective diagnosis of AD is critical for the development and delivery of drug treatments and/or interventions. Pathological changes in the medial temporal lobe (MTL) may occur several years prior to the onset of subjective memory complaints and diagnosis in the clinic (Sperling et al., 2011). The goal of the current work is to identify structural MTL measurements that indicate AD susceptibility in an ostensibly cognitively healthy community sample of older adults. Critically, in addition to the hippocampal subfields, this study investigated MTL cortex subregions that develop AD pathology (cellular loss, tau abnormalities, and tangle pathology) at the earliest stage of the disease (Jack and Holtzman, 2013; Jack et al., 2013, 2010).

Neuropsychological testing is necessary for the diagnosis of Mild Cognitive Impairment (MCI), a condition which often progresses to AD (Petersen, 2004; Sperling et al., 2011). The Montreal Cognitive Assessment (MoCA) is a brief neuropsychological screening tool that demonstrates excellent sensitivity and specificity in detecting MCI (Markwick et al., 2012; Nasreddine et al., 2005) and predicting future conversion to AD (Julayanont et al., 2014). Older adults who performed poorly on the MoCA also exhibited cognitive impairments in memory (D'Angelo et al., 2016; Yeung et al., 2013), have shown abnormal electrophysiological signatures (Newsome et al., 2013), and demonstrated similarly impaired performance on visual discrimination tasks as MCI patients (Newsome et al., 2012). The current investigation employed detailed volumetric analyses to investigate brain atrophy associated with poor MoCA performance in a group of community-dwelling older adults who, critically, have no current subjective memory complaints and no MCI diagnosis.

Advanced AD is associated with distributed neocortical structural changes (Scahill et al., 2002; Thompson et al., 2003); however the earliest stages of the disease are thought to develop within the MTL (Braak and Braak, 1991). Specific subregions of the MTL, including the entorhinal cortex (ERC; (Gómez-Isla et al., 1996; Krumm et al., 2016; Whitwell et al., 2007) and the CA1 subfield of the hippocampus (Chételat et al., 2008; de Flores et al., 2015; Gerardin et al., 2009; Iglesias et al., 2015; Kerchner et al., 2012; La Joie et al., 2013; Mueller and Weiner, 2009; Mueller et al., 2010a; Pluta et al., 2012; Tang et al., 2014; Yassa et al., 2010b; Yushkevich et al., 2015b) exhibit volumetric decreases in individuals with MCI.

The lateral portion of entorhinal cortex and the perirhinal cortex (PRC) were recently identified as a primary sites of cerebral blood volume (CBV) reductions in a group of 12 humans who subsequently developed AD (Khan et al., 2014). Similar CBV reductions were observed in the corresponding regions in transgenic mouse models of AD, suggesting that the lateral ERC and the PRC are affected earliest by AD pathology (Khan et al., 2014). Asymptomatic individuals with AD genetic risk, as well as preclinical healthy participants who demonstrated evidence of cerebral amyloid, were shown to have reductions in hippocampal and MTL cortical subregions, including the ERC, and medial PRC, indicating that disease-related structural atrophy can precede subjective memory complaints (Fox et al., 1996; Harrison et al., 2016; Wolk et al., 2016). However, to our knowledge, there has been no investigation of volumetric changes to the ERC within the ERC subregions; here we provide the first study to employ manual segmentation of the anterolateral ERC (alERC) and posteromedial ERC (pmERC) as a distinct subregions in contrast to examining the ERC as a whole, using a segmentation protocol derived from high-resolution functional connectivity analyses of the ERC (Maass et al., 2015).

We hypothesized that older adults who reported no subjective memory impairments, as assessed by the Memory Functioning Questionnaire (Gilewski et al., 1990), but nonetheless scored below the recommended cutoff MoCA score (<26) would have reduced volume in the MTL, specifically within the alERC, PRC, and the CA1 subfield of the hippocampus. To our knowledge only two studies have examined the relationship between MoCA performance and brain volumes, and within the MTL, these studies focused on the hippocampus proper (Gupta et al., 2015; Paul et al., 2011), which develops AD pathology later than the adjacent alERC (Braak and Braak, 1991). This is the first study to address the relationship between cognitive status, as assessed by the MoCA, and MTL subregional volumes. While the primary investigation focused on the MTL, global estimates of brain volume (total grey matter, white matter, and cerebrospinal fluid) were also investigated to determine whether cognitive decline was associated with these more global measures (Gupta et al., 2015). Finally, to rule out undetected stroke and investigate potential contributions of vascular pathology to cognitive impairment, volumetric assessment of white matter hyperintensities (WMH) was conducted (Brickman et al., 2015).

2 Material and methods

2.1 Participants

Forty community-dwelling, older adult participants (30 female; mean age=71.4 years, range=59-81, mean education=16.3 years, range=12-23) were recruited from participant databases at the RRI/Baycrest and the University of Toronto. All participants received the MoCA (Nasreddine et al., 2005), and were selected to create two age-matched groups that differed solely on the basis of their MoCA score (Figure 1). A score of 26 is the recommended threshold score for primary care physicians to provide further dementia screening (Damian et al., 2011); thus, the two groups were defined as an “at-risk” group (N=20; 17 female; mean age=72.5 years, range=59-81, mean education=16.2 years, range=12-22) who scored below 26 (indicating potentially pathological cognitive impairment and risk for MCI, mean score=23.4, range=17-25), and a “healthy” group (N=20; 13 female; mean age=70.3 years, range=63-77, mean education=16.6 years, range=12-23) who scored 26 and above (mean score=27.9, range=26-30). T-tests showed no difference between the two groups in age, $t(38)=1.29$, $p=.20$, or years of education, $t(38)=.51$, $p=.61$, but a significant difference in MoCA score, $t(38)=7.87$, $p<.001$.

All participants were fluent English speakers with normal or corrected-to-normal vision, and were screened for non-MRI compatible metal implants, color blindness, diabetes, neurological disorders, stroke, or brain trauma. All participants were informed about the nature of the experiment and its risks, and gave written informed consent. The Research Ethics Board of the University of Toronto and the RRI approved this research. All participants received monetary compensation for participation, following standard practices at the RRI.

2.2 Neuropsychological Battery

All participants received a battery of neuropsychological tests (Osterrieth, 1944; Reitan and Wolfson, 1985; Warrington and James, 1991; Wechsler, 2009, 1999; Wechsler et al., 2008) to characterize cognitive performance (Table 1). The magnitude of subjective memory complaints in everyday memory functioning was also quantified using the Memory Functioning Questionnaire (MFQ) to evaluate whether participants in either group had self-awareness of memory difficulties (Gilewski et al., 1990). The MFQ consists of 64 questions that probe frequency and seriousness of forgetting in daily life.

Participants responded using a 7-point Likert scale in which lower scores were associated with frequent forgetting and serious issues with forgetting and higher scores were associated with no forgetting and no serious issues with forgetting. In the current manuscript, responses are averaged across the 64 questions.

Neuropsychological testing was completed in a separate session prior to the MRI scan ($M=3$ months; $SD=5.5$ months). Results are presented in Table 1 along with effect sizes for the group differences. Overall, both groups of participants performed in the low-average to high-average range on neuropsychological tests of delayed memory, working memory, executive function, semantic memory, and visuospatial perception. However, when directly comparing the at-risk group to the healthy group, medium to large effects sizes on several standardized tests of delayed memory were observed. These included the WMS Logical Memory tests (delayed recall and recognition) and the Rey–Osterrieth delayed recall test. The at-risk group also demonstrated lower scores on tests of working memory (WAIS digit span), executive function (Trails A & B), and semantic memory (WASI vocabulary). Visuospatial performance was largely intact.

Scores on the MFQ were equivalent among the groups (Figure 1), and the scores obtained indicated that neither group self-reported significant functional memory difficulties outside of the laboratory. Although the at-risk individuals performed below the MoCA cut-off, these individuals did not report significant concerns about their memory, and performed, for the most part, in the average range on standard neuropsychological tests. In terms of objective memory impairments, none of the 20 individuals in the at-risk group scored within the impaired range on the WMS Logical Memory tests, whereas one of 20 participants in the healthy group scored in the impaired range on Logical Memory Immediate recall (Logical Memory I on Figure 1). On the Rey–Osterrieth delayed recall test, four of the 20 participants in the at-risk group and two out of the 20 in the healthy group scored in the impaired range (see Figure 1). Only two at-risk participants demonstrated impaired scores on executive function/short term memory (Digits Backward) and one was impaired on WASI vocabulary.

While none of the participants in our group have received a diagnosis of MCI, and none of these individuals expressed significant concerns about his/her memory based on their responses on the MFQ,

we cannot rule out the possibility that some of these individuals have declined cognitively and have poor insight, or were not forthcoming about their subjective memory concerns. It is possible that for some of the individuals in our at risk group, information about cognitive change obtained from an informant might allow for a diagnosis of MCI (Albert et al., 2011). However, in the absence of this information, and given their relatively good performance on the objective measures of memory and cognition, we refer to this group as demonstrating a potentially pathological cognitive impairment (based on their MoCA performance) and are at risk for MCI.

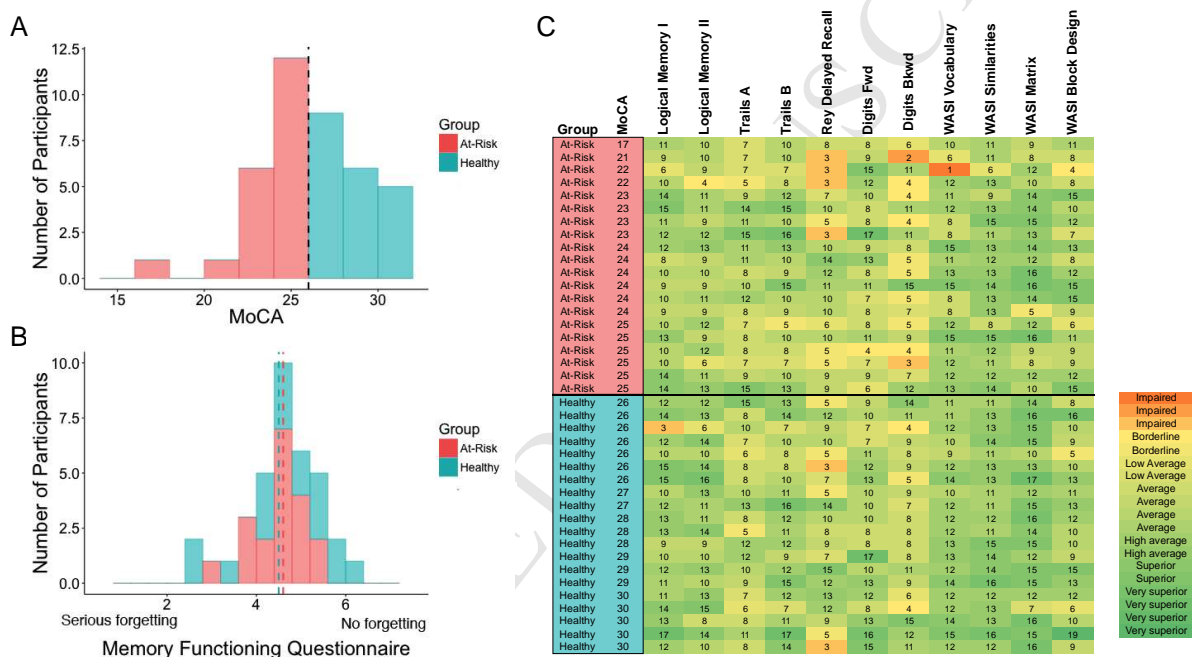


Figure 1. MoCA distribution and neuropsychological profile of current cohort. A: Distribution of MoCA scores in the current cohort. Black dashed line indicates the recommended MoCA cut-off score (26 points out of 30). B: Distribution of mean scores on the Memory Functioning Questionnaire (MFQ). Scores on the questionnaire correspond to the participants' self reported memory concerns (using a 7-point Likert scale). The two groups reported similar ratings on the MFQ (healthy: $M=4.6$, $SD=1.1$; at-risk: $M=4.5$, $SD=0.6$). C: Neuropsychological scaled scores colour coded to demonstrate that the only a handful of scores (in both at-risk and healthy groups) fall in the impaired range (orange boxes). Scaled scores were obtained from Fastenau and colleagues (1999) for the Rey-Osterrieth Complex Figure test and from the published manuals for all other tests.

2.3 Structural Image Acquisition

All neuroimaging was done on a 3T Siemens Trio scanner using a 12-channel head coil. Participants received a T1-weighted magnetization-prepared, rapid acquisition with gradient echo image (MP-RAGE) whole-brain anatomical scan (TE/TR=2.63 ms/2000ms, 160 axial slices perpendicular to the AC-PC line, 256x192 acquisition matrix, voxel size=1x1x1 mm, FOV=256mm). The MP-RAGE scan was used to obtain measures of brain and head size, as well as for the quantification of global grey and white matter and cerebral spinal fluid (CSF). The MP-RAGE scan was also used for slice placement during the acquisition of a subsequent high-resolution T2-weighted scan in an oblique-coronal plane, perpendicular to the hippocampal long axis (TE/TR=68ms/3000ms, 20-28 slices depending on head size, 512x512 acquisition matrix, voxel size=0.43x0.43x3 mm, no skip, FOV=220mm). For the high-resolution, T2-weighted scan, the first slice was placed anterior of the collateral sulcus (including the temporal pole where possible), and the last slice placed posterior to the hippocampal tail, to ensure full coverage of the entire hippocampus and MTL cortices for all participants. A whole-brain fluid-attenuated inversion recovery image (FLAIR; TE/TR=97/9000ms, 30-32 axial slices perpendicular to the AC-PC line, voxel size=0.875x0.875x5mm, 212x256 acquisition matrix, FOV=220mm, TI=2500ms) was collected to check for the presence of strokes and WMH.

Table 1. Neuropsychological Battery

Test	Healthy Older Adults	At-risk Older Adults	Effect size of difference between groups (Cohen's d)	
MoCA (/30)**	27.9 (1.7) Normal range	23.4 (1.9) Impaired	2.49	
† Visuospatial/Executive (/5)	4.2 (1.0)	3.7 (0.9)	0.60	
Naming (/3)**	3.0 (0.2)	2.4 (0.7)	1.09	
Attention (/6)*	5.9 (0.4)	5.3 (0.9)	0.78	
Language (/3)	2.8 (0.4)	2.4 (0.8)	0.57	
Abstraction (/2)	1.9 (0.3)	1.8 (0.6)	0.33	
Memory (/5)**	4.1 (1.1)	2.1 (1.4)	1.57	
Orientation (/6)*	6.0 (0.0)	5.8 (0.6)	0.64	
WMS-IV LM Immediate Recall Scaled Score (/20)	11.9 (2.9) 70.6%ile	10.9 (2.3) 58.7%ile	0.40	
WMS-IV LM Delayed Recall Scaled Score (/20)*	11.8 (2.5) 68.3%ile	10.0 (2.2) 50.0%ile	0.76	
WMS-IV LM Recognition Accuracy**	86% (10%)	78% (9%)	0.88	
Trails A	42.7s (11.6s) 39.2%ile	43.6s (15.5s) 43.1%ile	0.07	
Trails B*	79.0s (30.5s) 63.3%ile	102.1s (36.7s) 51.7%ile	0.69	
Digit Span Forward Score [†] (/16)	10.9 (2.0) 61.1%ile	9.6 (2.2) 44.1%ile	0.60	
Digit Span Backward Score* (/14)	7.6 (2.2) 41.5%ile	6.0 (2.5) 24.5%ile	0.65	
Rey-Osterrieth Complex Figure				
Copy (/32)	26.8 (5.2) 26.3%ile	27.3 (5.9) 30.7%ile	0.09	
Immediate Recall (/32)	13.0 (6.8)	11.9 (6.6)	0.18	

	43.7%ile	39.4%ile		
Delayed Recall (/32)	12.0 (6.6) 39.3%ile	9.9 (6.4) 31.1%ile	0.32	
WASI Vocabulary (/80) [†]	62.3 (5.3) 74.9%ile	56.9 (12.1) 58.4%ile	0.58	
WASI Similarities (/48) [†]	37.7 (3.8) 80.2%ile	34.9 (5.6) 70.4%ile	0.60	
WASI Matrix Reasoning (/32)**	24.8 (4.7) 84%ile	19.4(7.5) 68.1%ile	0.86	
WASI Block Design (/71)	33.3 (15.1) 57.3%ile	27.8 (14.3) 52.7%ile	0.38	
VOSP Shape Detection (/20) (Cut-off score < 15)	19.4 (0.9) Pass	19.0 (1.3) Pass	0.31	
VOSP Incomplete Letters (/20)* (Cut-off score < 16)	19.6 (0.8) Pass	19.0 (0.8) Pass	0.70	
VOSP Dot Counting (/10) (Cut-off score < 8)	9.9 (0/3) Pass	9.7 (0.5) Pass	0.42	
VOSP Position Discrimination (/20) [†] (Cut-off score < 18)	19.7 (0.6) Pass	18.9 (2.1) Pass	0.54	
VOSP Number Location (/10)* (Cut-off score < 7)	9.7 (0.7) Pass	8.6 (2.0) Pass	0.70	
VOSP Cube Analysis (/10) (Cut-off score < 6)	9.7 (0.7) Pass	9.2 (1.6) Pass	0.40	
VOSP Silhouettes (/30) (Cut-off score < 15)	20.2 (5.2) Pass	19.8 (5.3) Pass	0.08	
VOSP Object Decision (/20) (Cut-off score < 14)	17.2 (1.9) Pass	16.4 (2.0) Pass	0.40	
VOSP Progressive Silhouettes (/20) (Cut-off score > 15)	10.0 (2.6) Pass	10.4 (3.5) Pass	0.12	
Subjective memory rating (MFQ, 7-point Likert scale)	4.6 (1.1) Minimal subjective forgetting	4.5 (0.6) Minimal subjective forgetting	0.11	

Note. Mean and standard deviation are listed for each group. Maximum and cut-off scores for tests indicated in parentheses in left column. WMS-IV LM = Wechsler Memory Scale, 4th Edition, Logical Memory subtest; WASI = Wechsler Abbreviated Scale of Intelligence; VOSP = Visual Object and Spatial Perception battery. [†] indicates a trend towards significant difference between

healthy and at-risk older adults at $p < .10$, *indicates a significant difference at $p < .05$, ** $p < .01$. All *t*-tests were two-tailed. Colour in right-most column corresponds to the effect size (light grey = small Cohen's *d*, dark grey = medium Cohen's *d*, black = large Cohen's *d*).

2.4 Global Brain Measure Estimation Using Automated Segmentation

Global estimates of cortical grey and cerebral white matter volume, CSF, and the estimated total intracranial Volume (eTIV) were obtained using FreeSurfer (version 5.3; <http://surfer.nmr.mgh.harvard.edu/>). The eTIV was used to correct MTL subregion and WMH volumes for head-size (as a proxy for intracranial volume; Buckner et al., 2004). The technical details of the volumetric segmentation procedures are described by Fischl and colleagues (Fischl et al., 2002).

WMH load was estimated using the LST toolbox version 1.2.3 (<http://www.applied-statistics.de/lst.html>), an automated tool for the segmentation of WMH in FLAIR images (Schmidt et al., 2012), which has recently been used to evaluate WMH load in patients diagnosed with probable AD (Morgen et al., 2015). We employed the lesion growth algorithm, which operates in native space using the following steps. First, FLAIR images were bias-corrected to remove MRI field inhomogeneities, next FLAIR images were coregistered to T1-weighted images and each tissue class (grey matter, white matter, CSF) was determined from the T1-weighted images. The distribution of FLAIR intensities for each tissue was then analyzed with the aim of detecting hyperintense outliers, indicating lesion voxels. According to their spatial location, the lesion voxels were categorized in three lesions belief maps (grey and white matter, CSF), which were summed into a single lesion belief map. This initial (conservative) lesion map, was set as a binary version of the GM belief map on which the default kappa threshold was applied ($k=.3$). Visual inspection of the lesion probability maps and their corresponding FLAIR images confirmed that the default kappa threshold was optimal for the current data. Finally, the lesion growth algorithm refined the lesion probability map as neighbouring voxels were iteratively analyzed and assigned to white matter, grey matter or lesion until no further voxels are assigned to lesions. The result was a lesion probability map for each subject that was transformed into binary maps using a threshold of .5. WMH volumes were then extracted from the binary maps.

2.5 Manual Segmentation of the MTL Subregions

Manual segmentation was performed on the T2-weighted images, in participants' native space, on the oblique-coronal plane perpendicular to the long axis of the hippocampus (Figure 2; in-plane resolution=0.43x0.43mm). A single rater (L.Y.), who was blind to MoCA score/group status, manually delineated three hippocampal subfields (CA1, a region combining dentate gyrus, CA2 and CA3 [DG/CA2/3], subiculum), and four MTL cortex subregions (alERC, posteromedial entorhinal (pmERC), PRC, and parahippocampal cortices (PHC)) in FSLview. A second rater (R.K.O.), who was also blind to MoCA score/group status, segmented the same regions to provide an index of inter-rater reliability (see below). This segmentation protocol is largely similar to the Olsen-Amaral-Palombo (OAP) protocol which has been used for previous volumetric investigations of the MTL (Olsen et al., 2013, 2009; Palombo et al., 2013; Yushkevich et al., 2015a). The OAP protocol includes two additional regions of interest, which

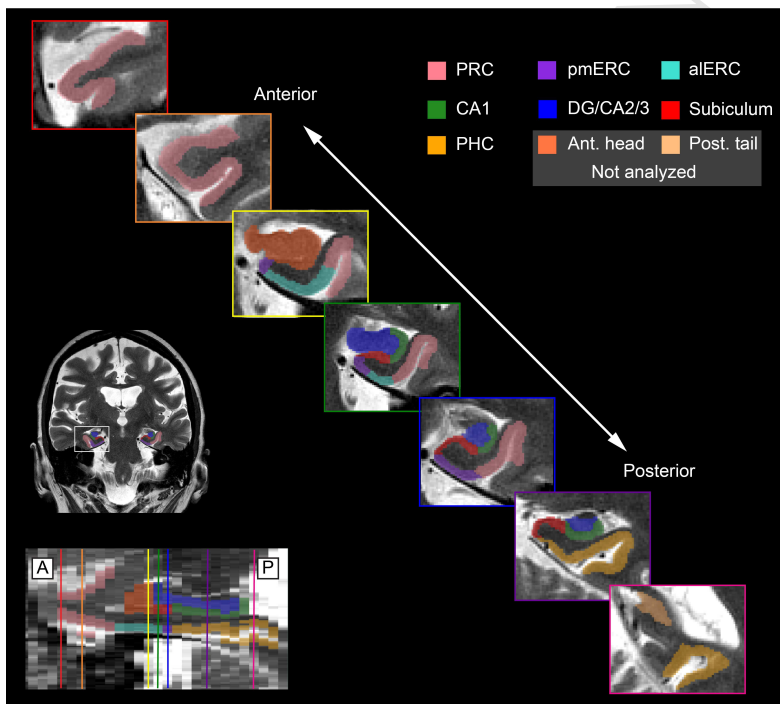


Figure 2. Segmentation protocol. Example coronal slices, spanning the anterior-posterior axis of the MTL. Slices depict the manual segmentation protocol used in the current study and regions of interest depict each of the seven regions (3 hippocampal subfields, 4 MTL cortex subregions) that were compared across groups. Note that the segmentation of the hippocampal subfields, perirhinal and parahippocampal cortices is the same protocol used in previous work (Olsen et al., 2013). The boundaries of the perirhinal cortex follow the depth rules defined by Insausti and colleagues (1998). The segmentation of the entorhinal cortex into anterolateral and posteromedial segments was adapted from the protocol of Maass, Berron and colleagues (2015).

cover the anterior head and the posterior tail of the hippocampus (orange and tan regions in Figure 2). There is currently little consensus as to how to subdivide these regions into subfields using *in vivo* 3 tesla MRI, which is why it has been our practice to combine them into a single region of interest, as do other high-resolution protocols (e.g. see Schlichting & Preston protocol in Yushkevich et al., 2015). Because the hippocampal subfields within these regions are not segmented into subregions, these regions were excluded from further analysis. The segmentation of the hippocampal subfields followed published anatomical atlases (Amaral and Insausti, 1990; Duvernoy, 2005). The segmentation of the MTL cortices followed the protocol of Insausti and colleagues for the ERC and PRC, and the protocol of Pruessner and colleagues for the PHC (Insausti et al., 1998; Pruessner et al., 2002). The lateral boundaries of the ERC and PRC were based on definitions established by Insausti and colleagues (1998). Specifically, when the collateral sulcus was “shallow” (depth < 1cm) the lateral extent of the ERC is drawn to the fundus of the collateral sulcus (see Figure 8 in Insausti et al., 1998) and the lateral boundary of the PRC is drawn to the midpoint between the lateral edge of the collateral sulcus and the medial edge of the occipitotemporal sulcus. When the collateral sulcus depth is “regular” (depth between 1 and 1.5 cm), the boundary between the ERC and PRC is drawn at the midpoint of the medial bank of the collateral sulcus and the lateral PRC border is drawn at the lateral edge of the collateral sulcus (see yellow-outlined slice in Figure 2). Finally, when the depth of the collateral sulcus is “deep” (depth \geq 1.5cm), the ERC and PRC boundary is defined by the medial edge of the collateral sulcus and the lateral border of the PRC is at the midpoint between the fundus and the lateral edge of the collateral sulcus (see green and blue outlined slices in Figure 2).

The subdivision of the entorhinal cortex into aERC and pmERC was adapted from the protocol of Maass, Berron and colleagues, which was derived from functional connectivity between the ERC, PRC and PHC (Maass et al., 2015). The protocol we used to define the entorhinal subregions was altered slightly to accommodate the thicker slices used in the current study and unlike the protocol used by Maas, Berron and colleagues, the lateral boundary of the aERC corresponds to the ERC definitions as defined by Insausti and colleagues (1998). We note that the lateral boundary of the aERC and pmERC regions here extend into the collateral sulcus when the depth of the collateral sulcus is “shallow” (depth <1 cm) or “regular” (depth between 1 and 1.5 cm), which means that the ERC subregions defined here overlap with

the transentorhinal region defined by Braak (Braak and Braak, 1992, 1991) and also with the medial PRC regions used in the literature (Krumm et al., 2016; Wolk et al., 2016).

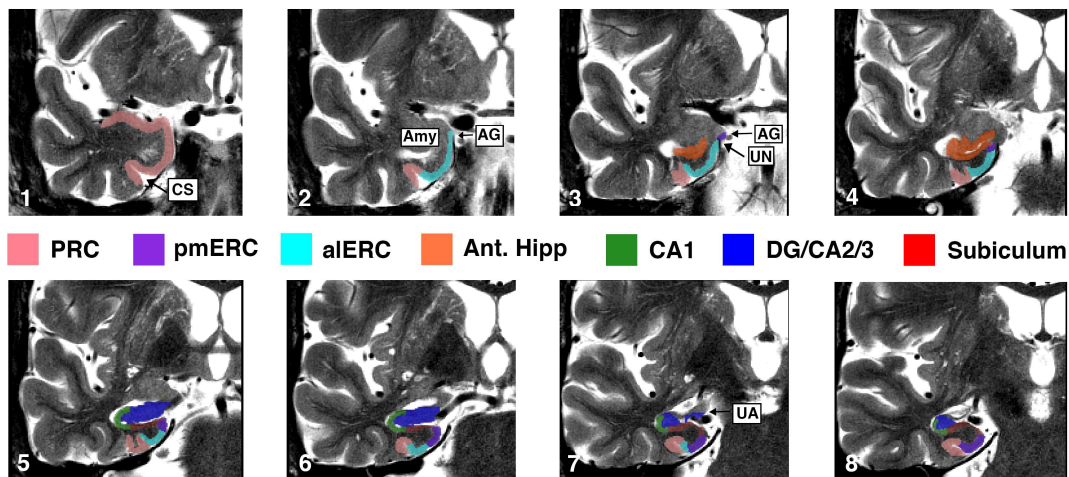


Figure 3. Segmentation protocol of ERC subregions with landmarks labeled These slices depict the boundaries between the alERC and pmERC in relation to surrounding MTL landmarks and collateral sulcus variation. Slice 1 depicts the MTL cortex anterior to the frontal-temporal junction, which contains PRC. In slice 2, the amygdala (Amy) and the frontotemporal junction are present and only the alERC is segmented. The dorsal/medial border of the alERC is drawn to the midpoint (usually the most medial section) of the gyrus ambiens (AG). The ventral/lateral alERC boundary is determined by the “depth” rules of Insausti et al., (1998). In slice 2, the depth of the collateral depth is “regular” and the alERC-PRC boundary is half-way up the medial bank of the collateral sulcus (CS). In slice 3, the hippocampal head is present, but it is “enclosed” in the white matter so the ERC does not connect to the hippocampal head. The dorsal/medial boundary of the pmERC is drawn from the most medial point of the AG and the ventral/lateral boundary is drawn to the uncal notch (UN). The ventral/lateral boundary of the alERC is drawn to the fundus of the CS on this slice because the CS is “shallow.” Note that the CS is bifurcated in slices 3-5, and the lateral boundary of PRC is drawn to the fundus of the more lateral CS. In slice 4, the subiculum in hippocampal head is now continuous with the parahippocampal gyrus and the ventral/lateral border of the pmERC is slightly inferior to the position on the previous slice and will continue to shift ventrolaterally on subsequent slices (slices 4 and 5). In slice 5, the C-shape structure within the “body-like” portion of the hippocampal head (formed by the CA1 subfield) can be visualized. On this slice, the boundary between the hippocampal head and pmERC falls at the “elbow” where the most superiomedial section of the parahippocampal gyrus meets the subiculum and covers the medial 1/3 of the ERC. As described by Maass, Berron and colleagues, the pmERC and alERC are approximately equal in size at the slice located at two-thirds of the anterior-posterior extent of the hippocampal head (slice 6). Slice 7 is located just anterior to the uncal apex (UA; uncus is still visible medially) and the uncus is absent in Slice 8. At the level of the UA (UA falls slightly posterior to Slice 7), the boundary between the alERC and pmERC is drawn closer to the boundary between the ERC and PRC, such that the pmERC covers the medial $\frac{3}{4}$ of the ERC and the alERC covers the lateral $\frac{1}{4}$ of ERC. In slice 8, which occurs just posterior to the last slice of the UA (the UA and/or gyrus intralimbicus is no longer visualized), only pmERC is present.

The division between the aERC and pmERC is as follows: at the most anterior aspect of the ERC (prior to the appearance of the hippocampus), only aERC is present (Figure 3, slice 2). According to Maass, Berron and colleagues, pmERC first appears approximately 2mm after the first appearance of the hippocampal head, and the aERC-pmERC border occurs at the uncal notch (sometimes referred to as the tentorial notch; see Ding and Van Hoesen, 2015). The uncal notch is an indentation formed mechanically by the free edge of the tentorium cerebelli (we refer the reader to Kivisaari et al., 2013, Figure 19.5 for an excellent visual depiction of this landmark). Accordingly, because the T2 scans used in the current study were 3mm thick in the anterior to posterior dimension, we designated the first slice of the pmERC on the first (most anterior) slice that contains hippocampal head (Figure 3, slice 3). On this slice, the pmERC is drawn from the most medial point of the gyrus ambiens ventrally to the uncal notch. Moving posteriorly, the boundary between the pmERC and aERC moves ventrally. When the shape of the lateral hippocampal head demonstrates a body-like structure (i.e. the CA1 subfield demonstrates a C-shape as in the body), the hippocampal subfields are segmented and the pmERC covers the medial 1/3 of the ERC (Figure 3, slice 5). Moving posteriorly, at slices located at two-thirds of the anterior-posterior extent of the hippocampal head, aERC and pmERC are approximately equivalent in size (see Figure 2, slice outlined in green and Figure 3, slice 6). At the level of the uncal apex (see Figure 1 of Poppenk et al., 2013), the boundary between the aERC and pmERC is drawn closer to the boundary between the ERC and PRC, such that the pmERC covers the medial $\frac{3}{4}$ of the ERC and the aERC covers the lateral $\frac{1}{4}$ of ERC. Note that depending on the neuroanatomy of the participant and/or slice placement of the image, the uncal apex itself might not be visualized (see Figure 3, slices 7 and 8). In this case, the last slice that contains uncal tissue will determine the placement of this final pmERC/aERC border, in which pmERC covers the medial $\frac{3}{4}$ of the ERC and the aERC covers the lateral $\frac{1}{4}$ of ERC. Finally, on the last ERC slice, which occurs just posterior to the last slice of the uncal apex (i.e. moving anterior to posterior, this is the first slice on which the uncal apex and/or gyrus intralimbicus is no longer visualized), only pmERC is present (see blue outlined slice in Figure 2 and Figure 3, slice 8).

2.6 MTL Manual Segmentation Reliability

Intra-rater reliability was established by comparing segmentation of five randomly selected scans, completed by the same rater (L.Y.) after a delay of 1-4 months. Inter-rater reliability was evaluated by comparing the segmentation of five randomly selected scans by a second rater (R.K.O) to those of L.Y. Reliability was assessed using the Intra-class correlation coefficient (ICC, which evaluates volume reliability) and the Dice metric (which also takes spatial overlap into account), computed separately for each region in each hemisphere (Dice, 1945; Shrout and Fleiss, 1979).

Table 2 – Reliability measurements

Subregion	Intra-rater: Dice		Intra-rater ICC		Inter-rater: Dice		Inter-rater: ICC	
	Left	Right	Left	Right	Left	Right	Left	Right
CA1	0.88	0.87	0.94	0.95	0.74	0.66	0.92	0.91
Subiculum	0.85	0.84	0.89	0.88	0.67	0.66	0.81	0.85
DG/CA2/3	0.91	0.90	0.94	0.99	0.75	0.73	0.91	0.96
alERC	0.86	0.85	0.96	0.86	0.72	0.73	0.87	0.71
pmERC	0.82	0.80	0.90	0.86	0.59	0.64	0.95	0.80
PRC	0.87	0.89	0.98	0.91	0.74	0.76	0.98	0.99
PHC	0.86	0.84	0.89	0.95	0.71	0.77	0.86	0.96

Note. Dice was computed for both intra- and inter-rater agreement. ICC(3,k) was calculated for intra-rater and ICC(2,k) was computed for inter-rater reliability.

ICC(3,k) was computed for intra-rater reliability (consistency) and ICC(2,k) was computed for inter-rater reliability (agreement). Dice was derived using the formula $2 \times (\text{intersecting region}) / (\text{original segmentation} + \text{repeat segmentation})$; a Dice overlap metric of 0 represents no overlap, whereas a metric of 1 represents perfect overlap. Intra-rater and inter-rater reliability results (Table 2) were comparable to reliability values reported in the literature for manual segmentation of hippocampal subfields and MTL cortices (Wisse et al., 2012; Yushkevich et al., 2015b) and are consistent with our previous work (Olsen et al., 2013; Palombo et al., 2013).

2.7 Statistics

Group differences were evaluated with t-tests and repeated measures ANOVAs in SPSS (version 22; IBM SPSS Statistics for Windows) Given the extensive literature reporting volume reductions in these regions as a function of AD severity (Adachi et al., 2003; Kerchner et al., 2012, 2010; La Joie et al., 2013; Mueller and Weiner, 2009; Mueller et al., 2010b, 2007; Pluta et al., 2012; Wisse et al., 2014; Yassa et al., 2010b), and our previous work on a similar group of individuals who demonstrated neural and behavioural impairments (D'Angelo et al., 2016; Newsome et al., 2013, 2012; Yeung et al., 2013), we had strong a priori hypotheses that brain volumes would be smaller in the at-risk group; thus, one-tailed tests were used when comparing both global and MTL regions. The three hippocampal subfields and four MTL cortical subregions were entered into a single ANOVA model to test for main effects of group and group by region interactions; significant interactions were followed up with independent t-tests. A second model, which included age as a covariate, was also run to control for small (non-significant) age differences between groups. The Holm-Bonferroni method was used to control familywise error rate when performing multiple comparisons. While primary analyses focused on the relationship between MTL volumes and cognitive status by treating MoCA performance as a categorical variable (i.e. pass/fail), supplementary analyses examined the nature of this underlying relationship between MTL volumes and MoCA score treated as a continuous variable. To characterize the relationship between brain volume and cognitive performance on the MoCA, bivariate correlations were calculated between MoCA and the volume of brain regions that demonstrated medium to large group differences (effect size measured using Cohen's d).

3 Results

3.1 Global Neuroimaging Measurements

Estimates of eTIV, cortical grey matter volume, cerebral white matter volume, and CSF for each group were compared for each group. No significant group differences were observed for the eTIV, cortical grey matter and CSF volume measures, and only a marginal difference was observed for cerebral white matter (Supplementary Table 1; $p > .08$). WMH volume for each group was also examined and a marginal group difference was observed ($t(38)=1.48$, $p=.08$). Visual examination of the FLAIR images ruled out the presence of previously undetected stroke.

3.2 Group Differences in MTL Subregion Volumes

A repeated-measures ANOVA was performed with brain region as a within-subjects factor, and group [at-risk, healthy] as a between-subject factor. Initial exploration of the data revealed no significant group X hemisphere interactions; consequently, the reported analyses were run on left and right hemispheres averaged. Mauchly's test indicated that the assumption of sphericity had been violated for the effect of brain region ($\chi^2(2)=279.52$, $p<.001$). Therefore, degrees of freedom were corrected using Greenhouse-Geisser estimates of sphericity ($\epsilon=0.30$).

There were significant main effects of brain region, $F(6,228)=404.27$, $p<.001$, $\eta^2=0.91$, and group, $F(1,38)=6.19$, $p=.02$, $\eta^2=.14$, and a marginal brain region x group interaction, $F(6,228)=2.57$, $p=.09$, $\eta^2=.06$. When age was added to the statistical model as a covariate, there was still a significant effect of brain region: $F(6, 222) = 4.70$, $p=.016$, $\eta^2=.11$, a significant effect of group ($1,37) = 4.51$, $p=.04$, $\eta^2=.11$, and a non-significant brain region x group interaction, $F(6,222)=2.30$, $p=.11$, $\eta^2=.06$.

The mean volumes (and SD, in mm^3) of each of the three hippocampal subfields and four MTL cortex subregions, in the at-risk and healthy groups are listed in Supplementary Table 2; boxplots for each region are plotted in Figure 4. Follow-up independent samples t-tests showed that only the aIERC region was significantly larger in the healthy versus the at-risk group ($t(38)=3.37$, $p=.001$), when accounting for multiple comparisons. The CA1 subfield ($t(38)=2.40$, $p=.01$), the perirhinal cortex ($t(38)=2.04$, $p=.02$) also showed group differences; however, these effects did not survive correction for multiple comparisons.

3.3 Relationship Between Overall MoCA Performance and MTL Volumes Across Participants

The primary analyses reported above examined volumes according to cognitive status, specified as a categorical variable (i.e. comparing the healthy and at-risk groups). Supplementary analyses were conducted on regions that demonstrated medium to large effect sizes in the primary analyses to illustrate the underlying profile of volume differences across the entire cohort as a function of MoCA score. In order to evaluate the nature of the relationship between structural atrophy in the MTL subregions and MoCA performance, linear regressions between MoCA score and MTL volumes were conducted (see

Supplementary Figure 1), and positive linear relationships between MTL volumes and MoCA score across the entire cohort were observed, even when age was added to the regression models.

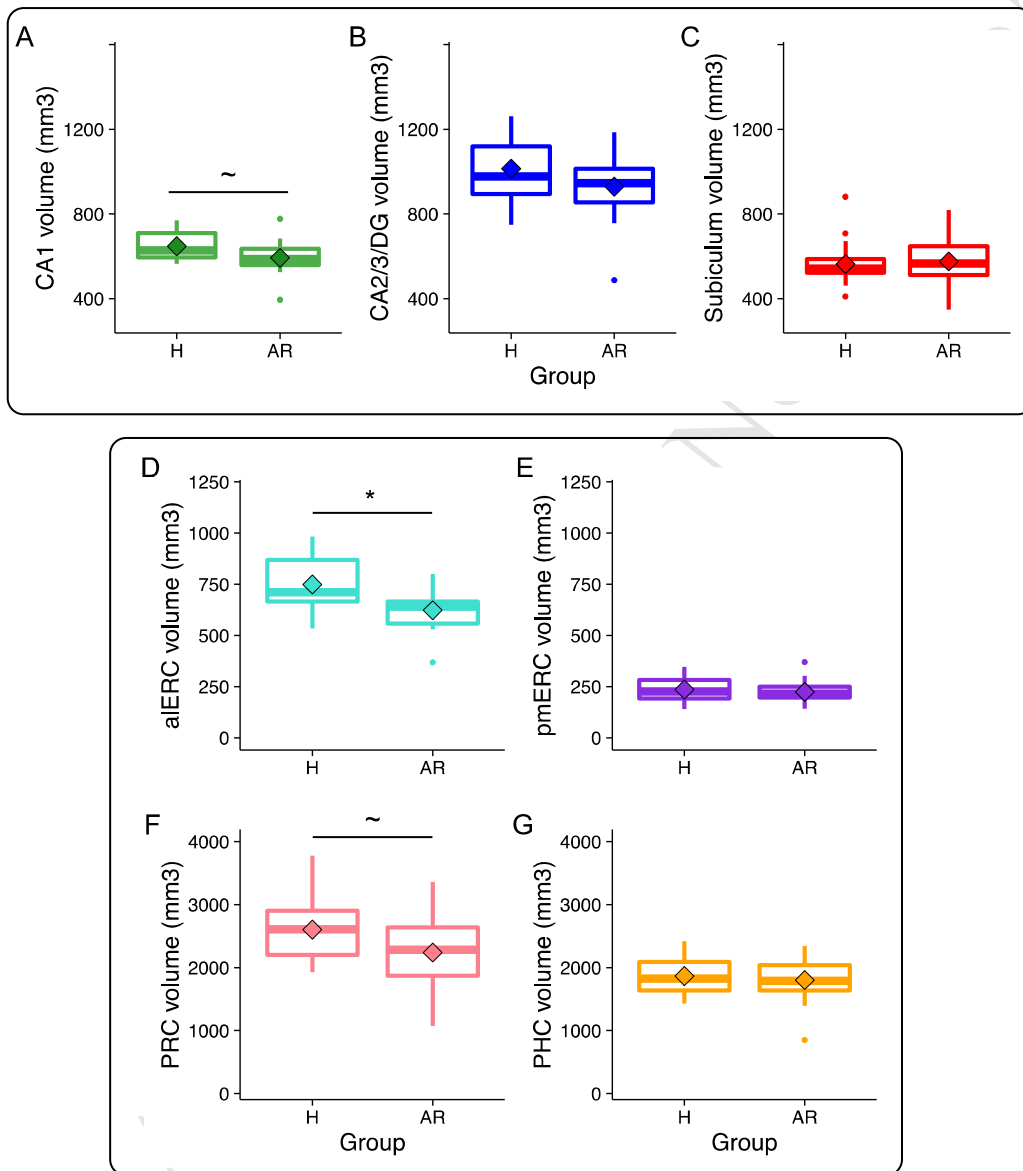


Figure 4. Hippocampal subfields and MTL cortical volumes. Box plots, plotted separately for healthy (H) and at-risk (AR) participants, for the hippocampal subfields (A-C) and MTL cortical subregions (D-G). ~Indicates a significant difference at $p < .05$ (does not survive multiple comparisons), * $p < .01$.

4. Discussion

We investigated MTL subregion volumes associated with cognitive decline in an ostensibly cognitively healthy older adult group. These undiagnosed individuals reported no subjective memory complaints as assessed by the MFQ but nonetheless scored below the recommended MoCA threshold, indicating that these individuals were at risk for developing dementia. Compared to the healthy group, our primary analyses found a significant volume reduction for the at-risk group in the aERC, a region implicated in the early stages of AD. The significant positive relationship between aERC volume and MoCA score was also observed in our supplementary analyses when MoCA was treated as a continuous, rather than a categorical variable, and when controlling for the effect of age. These results are important and novel for two reasons.

First, to our knowledge, this is the first study to employ segmentation of the aERC as a distinct region from the ERC as a whole, and thus we provide novel findings that link aERC volume to cognitive impairment. Combined with recent research suggesting that AD pathology originates from the lateral ERC (Khan et al., 2014), the extensive body of work which has shown overall volume reductions in the ERC as a function of MCI or AD status (Augustinack et al., 2012; Bobinski et al., 1999; Du et al., 2003, 2001; Fennema-Notestine et al., 2009; Fjell et al., 2014; Fujishima et al., 2014; Juottonen et al., 1998; Kerchner et al., 2013; Killiany et al., 2002; McDonald et al., 2009; Pennanen et al., 2004; Wisse et al., 2014), and work in healthy older adults which has indicated ERC-hippocampal structural connectivity is related to cognitive status (Yassa et al., 2010a), we propose that low aERC volume may be an early biomarker for AD risk.

While the MoCA results and selective aERC volume reductions in our at-risk group suggest that these individuals may have incipient AD pathology, despite the fact that they have not been diagnosed with MCI or even reported a serious cognitive concern. A particularly striking aspect of these findings is that the individuals in the at-risk group for the most part scored in the average range on standard neuropsychological tests, including those probing episodic memory (Figure 1). Furthermore, participants did not report being worried about changes in their memory, although it is possible that some participants could have poor insight or were not forthcoming about experiencing cognitive changes. In future studies we would like to examine these individuals for the presence of AD biomarkers such as amyloid-beta (or

tau) in the CSF, using amyloid/tau PET tracers, and/or a formal neuropsychological diagnosis with longitudinal follow-up. These prospective/longitudinal studies are necessary to determine whether aERC volume is a sensitive and specific marker for AD.

Second, this is the first study to directly show that lower MoCA scores are related to volumes in specific MTL subregions that are affected in AD. While the MoCA has been shown to have a high specificity and selectivity for cognitive impairment, only two studies have previously examined the relationship between the MoCA and brain volume (Gupta et al., 2015; Paul et al., 2011) and neither of these studies looked specifically at MTL cortical subregions or hippocampal subfields. Our findings show that reduced aERC volumes, and to a lesser extent, reduced CA1 and PRC volumes, precede subjective memory complaints in community-dwelling individuals, and further support the use of the MoCA as a predictive measure for AD (Julayanont et al., 2014; Nasreddine et al., 2005).

Recent work examining the relationship between global neuroimaging measurements and MoCA score reported significant associations between overall grey matter volume and CSF with cognitive performance (Gupta et al., 2015). In the current study, however, global neuroimaging measurements did not demonstrate significant group differences.

It is important to note that the nomenclature used to describe the regions of the anterior MTL cortex is quite variable in the extant literature, and we will note that the area originally described by Braak and Braak (1991) as the transentorhinal cortex has been referred to as both lateral ERC (e.g. Khan et al., 2015) and medial PRC (e.g. Wolk et al. 2016). However, Braak and Braak defined the transentorhinal region as a separate transition region that is a neuroanatomically distinct region of both ERC and PRC, and care should be taken when describing these regions. While there is currently little consensus among neuroanatomists regarding a definitive characterization of the ERC subregions (Yassa et al., 2014), this work provides evidence that parcellation of the ERC into its anterolateral and posteromedial subregions provides a useful characterization of the MTL regions affected by cognitive decline. We are unaware of data on the anterior-posterior distribution of the transentorhinal cortex; however, the aERC definition used in the current manuscript is largely overlapping with the visual depiction of the transentorhinal region provided by Braak and Braak (1991).

In conclusion, this is the first study to show reduced aERC volumes in ostensibly cognitively healthy individuals who scored poorly on the MoCA, suggestive of AD-related cognitive decline, in the absence of any group differences in global brain volume or WMH. Importantly, the aERC is the brain region in which AD pathology is believed to originate (Yassa, 2014), and the reductions observed here may reflect early AD pathology. This research reveals a potentially sensitive imaging biomarker of pathological aging, and provides a neural target for early screening, evaluation of disease progression, and intervention efficacy.

Acknowledgments:

This work was supported by grants from the Canadian Institutes of Health Research (CIHR) to MDB (grant number MOP-115148) and JDR (grant number MOP-126003). MDB and JDR are supported by Canada Research Chairs. MDB is also supported by a Scholar Award from the James S McDonnell Foundation. L-KY is supported by a Natural Sciences and Engineering Research Council (NSERC) Canadian Graduate Scholarship. We would like to thank Dr. Nicole D. Anderson, a trained neuropsychologist, who provided her clinical judgment regarding the presence of possible objective cognitive memory impairments in our at-risk group.

References

- Adachi, M., Kawakatsu, S., Hosoya, T., Otani, K., Honma, T., Shibata, A., Sugai, Y., 2003. Morphology of the inner structure of the hippocampal formation in Alzheimer disease. *Am. J. Neuroradiol.* 24, 1575–1581.
- Amaral, D.G., Insausti, R., 1990. The hippocampal formation, in: Paxinos, G. (Ed.), *The Human Nervous System*. Academic Press, San Diego, CA.
- Augustinack, J.C., Huber, K.E., Postelnicu, G.M., Kakunoori, S., Wang, R., van der Kouwe, A.J.W., Wald, L.L., Stein, T.D., Frosch, M.P., Fischl, B., 2012. Entorhinal verrucae geometry is coincident and correlates with Alzheimer's lesions: a combined neuropathology and high-resolution ex vivo MRI analysis. *Acta Neuropathol.* 123, 85–96. doi:10.1007/s00401-011-0929-5
- Bobinski, M., de Leon, M.J., Convit, A., De Santi, S., Wegiel, J., Tarshish, C.Y., Saint Louis, L.A., Wisniewski, H.M., 1999. MRI of entorhinal cortex in mild Alzheimer's disease. *Lancet* 353, 38–40.
- Braak, H., Braak, E., 1992. The human entorhinal cortex: normal morphology and lamina-specific pathology in various diseases. *Neurosci. Res.* 15, 6–31. doi:10.1016/0168-0102(92)90014-4
- Braak, H., Braak, E., 1991. Neuropathological staging of Alzheimer-related changes. *Acta Neuropathol.* 82, 239–59. doi:10.1007/BF00308809
- Brickman, A.M., Zahodne, L.B., Guzman, V.A., Narkhede, A., Meier, I.B., Griffith, E.Y., Provenzano, F.A., Schupf, N., Manly, J.J., Stern, Y., Luchsinger, J.A., Mayeux, R., 2015. Reconsidering harbingers of dementia: Progression of parietal lobe white matter hyperintensities predicts Alzheimer's disease incidence. *Neurobiol. Aging* 36, 27–32. doi:10.1016/j.neurobiolaging.2014.07.019
- Buckner, R.L., Head, D., Parker, J., Fotenos, A.F., Marcus, D., Morris, J.C., Snyder, A.Z., 2004. A unified approach for morphometric and functional data analysis in young, old, and demented adults using automated atlas-based head size normalization: Reliability and validation against manual measurement of total intracranial volume. *Neuroimage* 23, 724–738. doi:10.1016/j.neuroimage.2004.06.018
- Chételat, G., Fouquet, M., Kalpouzos, G., Denghien, I., De la Sayette, V., Viader, F., Mézenge, F., Landeau, B., Baron, J.C., Eustache, F., Desgranges, B., 2008. Three-dimensional surface mapping of hippocampal atrophy progression from MCI to AD and over normal aging as assessed using voxel-based morphometry. *Neuropsychologia* 46, 1721–31. doi:10.1016/j.neuropsychologia.2007.11.037
- D'Angelo, M.C., Smith, V.M., Kacollja, A., Zhang, F., Binns, M.A., Barense, M.D., Ryan, J.D., 2016. The effectiveness of unitization in mitigating age-related relational learning impairments depends on existing cognitive status. *Aging, Neuropsychol. Cogn.* 5585, 1–24. doi:10.1080/13825585.2016.1158235
- Damian, A.M., Jacobson, S.A., Hentz, J.G., Belden, C.M., Shill, H.A., Sabbagh, M.N., Caviness, J.N., Adler, C.H., 2011. The Montreal cognitive assessment and the mini-mental state examination as screening instruments for cognitive impairment: Item analyses and threshold scores. *Dement. Geriatr. Cogn. Disord.* 31Da, 126–131. doi:10.1159/000323867
- de Flores, R., La Joie, R., Landeau, B., Perrotin, A., Mézenge, F., de La Sayette, V., Eustache, F., Desgranges, B., Chételat, G., 2015. Effects of age and Alzheimer's disease on hippocampal subfields: Comparison between manual and freesurfer volumetry. *Hum. Brain Mapp.* 36, 463–474. doi:10.1002/hbm.22640
- Dice, L.R., 1945. Measures of the amount of ecologic association between species. *Ecology* 26, 297–302.
- Ding, S.-L., Van Hoesen, G.W., 2015. Organization and detailed parcellation of human hippocampal head and body regions based on a combined analysis of Cyto- and chemoarchitecture. *J. Comp. Neurol.*

- 523, 2233–2253. doi:10.1002/cne.23786
- Du, A.T., Schuff, N., Zhu, X.P., Jagust, W.J., Miller, B.L., Reed, B.R., Kramer, J.H., Mungas, D., Yaffe, K., Chui, H.C., Weiner, M.W., 2003. Atrophy rates of entorhinal cortex in AD and normal aging. *Neurology* 60, 481–486.
- Du, A.T., Schuff, N., Amend, D., Laakso, M.P., Hsu, Y.Y., Jagust, W.J., Yaffe, K., Kramer, J.H., Reed, B., Norman, D., Chui, H.C., Weiner, M.W., Street, C., 2001. Magnetic resonance imaging of the entorhinal cortex and hippocampus in mild cognitive impairment and Alzheimer's disease. *J. Neurol.* 71, 441–447.
- Duvernoy, H.M., 2005. *The human hippocampus: functional anatomy, vascularization, and serial sections with MRI.* Springer, New York.
- Fastenau, P.S., Denburg, N.L., Hufford, B.J., Fastenau, P.S., Denburg, N.L., Adult, B.J.H., Fastenau, P.S., Denburg, N.L., Hufford, B.J., 1999. Adult Norms for the Rey-Osterrieth Complex Figure Test and for Supplemental Recognition and Matching Trials from the Extended Complex Figure Test Adult Norms for the Rey-Osterrieth Complex Figure Test and for Supplemental Recognition and Matching Trials. *Clin. Neuropsychol.* 13, 30–47.
- Fennema-Notestine, C., Hagler, D.J., McEvoy, L.K., Fleisher, A.S., Wu, E.H., Karow, D.S., Dale, A.M., 2009. Structural MRI biomarkers for preclinical and mild Alzheimer's disease. *Hum. Brain Mapp.* 30, 3238–53. doi:10.1002/hbm.20744
- Fischl, B., Salat, D.H., Busa, E., Albert, M., Dieterich, M., Haselgrove, C., Kouwe, A. Van Der, Killiany, R., Kennedy, D., Klaveness, S., Montillo, A., Makris, N., Rosen, B., Dale, A.M., 2002. Whole Brain Segmentation: Neurotechnique Automated Labeling of Neuroanatomical Structures in the Human Brain. *Neuron* 33, 341–355.
- Fjell, A.M., Westlye, L.T., Grydeland, H., Amlie, I., Espeseth, T., Reinvang, I., Raz, N., Dale, A.M., Walhovd, K.B., 2014. Accelerating cortical thinning: unique to dementia or universal in aging? *Cereb. Cortex* 24, 919–34. doi:10.1093/cercor/bhs379
- Fox, N.C., Warrington, E.K., Freeborough, P.A., Hartikainen, P., Kennedy, A.M., 1996. Presymptomatic hippocampal atrophy in Alzheimer's disease: A longitudinal MRI study. *Brain* 119, 2001–2007.
- Fujishima, M., Maikusa, N., Nakamura, K., Nakatsuka, M., Matsuda, H., Meguro, K., 2014. Mild cognitive impairment, poor episodic memory, and late-life depression are associated with cerebral cortical thinning and increased white matter hyperintensities. *Front. Aging Neurosci.* 6, 306. doi:10.3389/fnagi.2014.00306
- Gerardin, E., Chételat, G., Chupin, M., Cuingnet, R., Desgranges, B., 2009. *NeuroImage* Multidimensional classification of hippocampal shape features discriminates Alzheimer's disease and mild cognitive impairment from normal aging. *Neuroimage* 47, 1476–1486. doi:10.1016/j.neuroimage.2009.05.036
- Gilewski, M.J., Zelinsky, E.M., Schaie, K.W., 1990. The Memory Functioning Questionnaire for Assessment of Memory Complaints in Adulthood and Old Age. *Psychol. Aging* 5, 482–490.
- Gómez-Isla, T., Price, J.L., McKeel, D.W., Morris, J.C., Growdon, J.H., Hyman, B.T., 1996. Profound loss of layer II entorhinal cortex neurons occurs in very mild Alzheimer's disease. *J. Neurosci.* 16, 4491–4500.
- Gupta, M., King, K.S., Srinivasa, R., Weiner, M.F., Hulse, K., Ayers, C.R., Whittemore, A., Mccoll, R.W., Rossetti, H.C., Peshock, R.M., 2015. Association of 3.0-T Brain Magnetic Resonance Imaging Biomarkers With Cognitive Function in the Dallas Heart Study. *JAMA Neurol.* 72, 170–175. doi:10.1001/jamaneurol.2014.3418
- Harrison, T.M., Mahmood, Z., Lau, E.P., Karacozoff, A.M., Burggren, A.C., Small, G.W., Bookheimer, S.Y., 2016. An Alzheimers Disease Genetic Risk Score Predicts Longitudinal Thinning of

- Hippocampal Complex Subregions in Healthy Older Adults. *eNeuro*. doi:10.1523/ENEURO.0098-16.2016
- IBM SPSS Statistics for Windows, n.d.
- Iglesias, J.E., Augustinack, J.C., Nguyen, K., Player, C.M., Player, A., Wright, M., Roy, N., Frosch, M.P., McKee, A.C., Wald, L.L., Fischl, B., Van Leemput, K., 2015. A computational atlas of the hippocampal formation using ex vivo, ultra-high resolution MRI: Application to adaptive segmentation of in vivo MRI. *Neuroimage* 115, 117–137. doi:10.1016/j.neuroimage.2015.04.042
- Insausti, R., Jouttonen, K., Soininen, H., Insausti, A.M., Partanen, K., Vainio, P., Laakso, M.P., Pitka, A., 1998. MR Volumetric Analysis of the Human Entorhinal , Perirhinal , and Temporopolar Cortices. *Am. J. Neuroradiol.* 19, 659–671.
- Jack, C.R., Holtzman, D.M., 2013. Biomarker modeling of alzheimer's disease. *Neuron* 80, 1347–1358. doi:10.1016/j.neuron.2013.12.003
- Jack, C.R., Knopman, D.S., Jagust, W.J., Petersen, R.C., Weiner, M.W., Aisen, P.S., Shaw, L.M., Vemuri, P., Wiste, H.J., Weigand, S.D., Lesnick, T.G., Pankratz, V.S., Donohue, M.C., Trojanowski, J.Q., 2013. Update on hypothetical model of Alzheimer's disease biomarkers. *Lancet Neurol.* 12, 207–216. doi:10.1016/S1474-4422(12)70291-0.Update
- Jack, C.R., Knopman, D.S., Jagust, W.J., Shaw, L.M., Aisen, P.S., Weiner, W., Petersen, R.C., Trojanowski, J.Q., 2010. Hypothetical model of dynamic biomarkers of the Alzheimer's pathological cascade. *Lancet Neurol.* 9, 1–20. doi:10.1016/S1474-4422(09)70299-6.Hypothetical
- Julayanont, P., Brousseau, M., Chertkow, H., Phillips, N., Nasreddine, Z.S., 2014. Montreal Cognitive Assessment Memory Index Score (MoCA-MIS) as a predictor of conversion from mild cognitive impairment to Alzheimer's disease. *J. Am. Geriatr. Soc.* 62, 679–684. doi:10.1111/jgs.12742
- Jouttonen, K., Laakso, M.P., Insausti, R., Lehtovirta, M., Pitkänen, A., Partanen, K., Soininen, H., 1998. Volumes of the entorhinal and perirhinal cortices in Alzheimer's disease. *Neurobiol. Aging* 19, 15–22. doi:10.1016/S0197-4580(98)00007-4
- Kerchner, G.A., Bernstein, J.D., Fenesy, M.C., Deutsch, G.K., Saranathan, M., Zeineh, M.M., Rutt, B.K., 2013. Shared vulnerability of two synaptically-connected medial temporal lobe areas to age and cognitive decline: a seven tesla magnetic resonance imaging study. *J. Neurosci.* 33, 16666–72. doi:10.1523/JNEUROSCI.1915-13.2013
- Kerchner, G.A., Deutsch, G.K., Zeineh, M., Dougherty, R.F., Saranathan, M., Rutt, B.K., 2012. Hippocampal CA1 apical neuropil atrophy and memory performance in Alzheimer's disease. *Neuroimage* 63, 194–202. doi:10.1016/j.neuroimage.2012.06.048
- Kerchner, G.A., Hess, C.P., Hammond-Rosenbluth, K.E., Xu, D., Rabinovici, G.D., Kelley, D. a C., Vigneron, D.B., Nelson, S.J., Miller, B.L., 2010. Hippocampal CA1 apical neuropil atrophy in mild Alzheimer disease visualized with 7-T MRI. *Neurology* 75, 1381–1387. doi:10.1212/WNL.0b013e3181f736a1
- Khan, U.A., Liu, L., Provenzano, F.A., Berman, D.E., Profaci, C.P., Sloan, R., Mayeux, R., Duff, K.E., Small, S.A., 2014. Molecular drivers and cortical spread of lateral entorhinal cortex dysfunction in preclinical Alzheimer's disease. *Nat. Neurosci.* 17, 304–11. doi:10.1038/nn.3606
- Killiany, R.J., Hyman, B.T., Moss, M.B., Kikinis, R., Jolesz, F., Tanzi, R., Jones, K., Albert, M.S., 2002. MRI measures of entorhinal cortex vs hippocampus in preclinical AD 619–624.
- Kivisaari, S.L., Probst, A., Taylor, K.I., 2013. The Perirhinal, Entorhinal, and Parahippocampal Cortices and Hippocampus: An Overview of Functional Anatomy and Protocol for Their Segmentation in MR Images, in: Ulmer, S., Jansen, O. (Eds.), *fMRI: Basics and Clinical Applications*. Springer Berlin Heidelberg, Berlin, Heidelberg, pp. 239–267. doi:10.1007/978-3-642-34342-1

- Krumm, S., Kivisaari, S.L., Probst, A., Monsch, A.U., Reinhardt, J., Ulmer, S., Stippich, C., Kressig, R.W., Taylor, K.I., 2016. Cortical thinning of parahippocampal subregions in very early Alzheimer's disease. *Neurobiol. Aging* 38, 188–196. doi:10.1016/j.neurobiolaging.2015.11.001
- La Joie, R., Perrotin, A., de La Sayette, V., Egret, S., Dœuvre, L., Belliard, S., Eustache, F., Desgranges, B., Chételat, G., 2013. Hippocampal subfield volumetry in mild cognitive impairment, Alzheimer's disease and semantic dementia. *NeuroImage Clin.* 3, 155–162. doi:10.1016/j.nicl.2013.08.007
- Maass, A., Berron, D., Libby, L. a, Ranganath, C., Düzel, E., 2015. Functional subregions of the human entorhinal cortex. *Elife* 4, 1–20. doi:10.7554/eLife.06426
- Markwick, A., Zamboni, G., de Jager, C. a., 2012. Profiles of cognitive subtest impairment in the Montreal Cognitive Assessment (MoCA) in a research cohort with normal Mini-Mental State Examination (MMSE) scores. *J. Clin. Exp. Neuropsychol.* 34, 750–757. doi:10.1080/13803395.2012.672966
- Mcdonald, C.R., Mcevoy, L.K., Gharapetian, L., Brewer, J.B., Dale, A.M., 2009. Regional rates of neocortical atrophy from normal aging to early Alzheimer disease 457–465.
- Morgen, K., Schneider, M., Frölich, L., Tost, H., Plichta, M.M., Kölsch, H., Rakebrandt, F., Rienhoff, O., Jessen, F., Peters, O., Jahn, H., Luckhaus, C., Hüll, M., Gertz, H., Schröder, J., Hampel, H., Teipel, S.J., Pantel, J., Heuser, I., Wiltfang, J., Rütger, E., Kornhuber, J., Maier, W., 2015. Apolipoprotein E-dependent load of white matter hyperintensities in Alzheimer ' s disease : a voxel-based lesion mapping study 1–14. doi:10.1186/s13195-015-0111-8
- Mueller, S.G., Schuff, N., Yaffe, K., Madison, C., Miller, B., Weiner, M.W., 2010a. Hippocampal atrophy patterns in mild cognitive impairment and Alzheimer's disease. *Hum. Brain Mapp.* 31, 1339–47. doi:10.1002/hbm.20934
- Mueller, S.G., Schuff, N., Yaffe, K., Madison, C., Miller, B., Weiner, M.W., 2010b. Hippocampal atrophy patterns in mild cognitive impairment and Alzheimer's disease. *Hum. Brain Mapp.* 31, 1339–1347. doi:10.1002/hbm.20934
- Mueller, S.G., Stables, L., Du, a T., Schuff, N., Truran, D., Cashdollar, N., Weiner, M.W., 2007. Measurement of hippocampal subfields and age-related changes with high resolution MRI at 4T. *Neurobiol. Aging* 28, 719–726. doi:10.1016/j.neurobiolaging.2006.03.007
- Mueller, S.G., Weiner, M.W., 2009. Selective effect of age, Apo e4, and Alzheimer's disease on hippocampal subfields. *Hippocampus* 19, 558–64. doi:10.1002/hipo.20614
- Nasreddine, Z.S., Phillips, N.A., Bedirian, V., Charbonneau, S., Whitehead, V., Collin, I., Cummings, J.L., Chertkow, H., 2005. The Montreal Cognitive Assessment, MoCA: a brief screening tool for mild cognitive impairment. *J. Am. Geriatr. Soc.* 53, 695–699. doi:10.1111/j.1532-5415.2005.53221.x
- Newsome, R.N., Duarte, A., Barense, M.D., 2012. Reducing perceptual interference improves visual discrimination in mild cognitive impairment: Implications for a model of perirhinal cortex function. *Hippocampus* 22, 1990–1999. doi:10.1002/hipo.22071
- Newsome, R.N., Pun, C., Smith, V.M., Ferber, S., Barense, M.D., 2013. Neural correlates of cognitive decline in older adults at-risk for developing MCI: Evidence from the CDA and P300. *Cogn. Neurosci.* 4, 152–162. doi:10.1080/17588928.2013.853658
- Olsen, R.K., Nichols, E.A., Chen, J., Hunt, J.F., Glover, G.H., Gabrieli, J.D.E., Wagner, A.D., 2009. Performance-related sustained and anticipatory activity in human medial temporal lobe during delayed match-to-sample. *J. Neurosci.* 29, 11880–11890. doi:10.1523/JNEUROSCI.2245-09.2009
- Olsen, R.K., Palombo, D.J., Rabin, J.S., Levine, B., Ryan, J.D., Rosenbaum, R.S., 2013. Volumetric analysis of medial temporal lobe subregions in developmental amnesia using high-resolution magnetic resonance imaging. *Hippocampus* 23, 855–60. doi:10.1002/hipo.22153
- Osterrieth, P.A., 1944. The test of copying a complex figure: A contribution to the study of perception and

- memory. *Arch. Psychol. (Geneve)*. 30, 286–356.
- Palombo, D.J., Amaral, R.S.C., Olsen, R.K., Müller, D.J., Todd, R.M., Anderson, A.K., Levine, B., 2013. KIBRA polymorphism is associated with individual differences in hippocampal subregions: evidence from anatomical segmentation using high-resolution MRI. *J. Neurosci.* 33, 13088–13093. doi:10.1523/JNEUROSCI.1406-13.2013
- Paul, R., Lane, E.M., Tate, D.F., Heaps, J., Romo, D.M., Akbudak, E., Niehoff, J., Conturo, T.E., 2011. Neuroimaging Signatures and Cognitive Correlates of the Montreal Cognitive Assessment Screen in a Nonclinical Elderly Sample 1–7. doi:10.1093/arclin/acr017
- Pennanen, C., Kivipelto, M., Tuomainen, S., Hartikainen, P., Hänninen, T., Laakso, M.P., Hallikainen, M., Vanhanen, M., Nissinen, A., Helkala, E.-L., Vainio, P., Vanninen, R., Partanen, K., Soininen, H., 2004. Hippocampus and entorhinal cortex in mild cognitive impairment and early AD. *Neurobiol. Aging* 25, 303–310. doi:10.1016/S0197-4580(03)00084-8
- Petersen, R.C., 2004. Mild cognitive impairment as a clinical entity and treatment target. *J. Intern. Med.* 256, 183–194. doi:10.1001/archneur.62.7.1160
- Pluta, J., Yushkevich, P.A., Das, S., Wolk, D., 2012. In vivo analysis of hippocampal subfield atrophy in mild cognitive impairment via semi-automatic segmentation of T2-weighted MRI. *J. Alzheimer's Dis.* 31, 85–99. doi:10.3233/JAD-2012-111931
- Poppenk, J., Evensmoen, H.R., Moscovitch, M., Nadel, L., 2013. Long-axis specialization of the human hippocampus. *Trends Cogn. Sci.* 17, 230–40. doi:10.1016/j.tics.2013.03.005
- Pruessner, J.C., Köhler, S., Crane, J., Lord, C., Byrne, A., Kabani, N., Collins, D.L., Evans, A.C., 2002. Entorhinal and Parahippocampal Cortex from High-resolution MR Images : Considering the Variability of the Collateral Sulcus. *Cereb. Cortex* 12, 1342–1353.
- Reitan, R.M., Wolfson, D., 1985. The Halstead-Reitan neuropsychological test battery: Theory and clinical interpretation. *Reitan Neuropsychology*.
- Scahill, R.I., Schott, J.M., Stevens, J.M., Rossor, M.N., Fox, N.C., 2002. Mapping the evolution of regional atrophy in Alzheimer ' s disease : Unbiased analysis of fluid-registered serial MRI. *Proc. Natl. Acad. Sci.* 99, 1–5.
- Schmidt, P., Gaser, C., Arsic, M., Buck, D., F??rschler, A., Berthele, A., Hoshi, M., Ilg, R., Schmid, V.J., Zimmer, C., Hemmer, B., M??hlau, M., 2012. An automated tool for detection of FLAIR-hyperintense white-matter lesions in Multiple Sclerosis. *Neuroimage* 59, 3774–3783. doi:10.1016/j.neuroimage.2011.11.032
- Shrout, P.E., Fleiss, J.L., 1979. Intraclass Correlations : Uses in Assessing Rater Reliability 86, 420–428.
- Sperling, R.A., Aisen, P.S., Beckett, L.A., Bennett, D.A., Craft, S., Fagan, A.M., Iwatsubo, T., Jack, C.R., Kaye, J., Montine, T.J., Park, D.C., Reiman, E.M., Rowe, C.C., Siemers, E., Stern, Y., Yaffe, K., Carrillo, M.C., Thies, B., Morrison-Bogorad, M., Wagster, M. V, Phelps, C.H., 2011. Toward defining the preclinical stages of Alzheimer's disease: Recommendations from the National Institute on Aging-Alzheimer's Association workgroups on diagnostic guidelines for Alzheimer's disease. *Alzheimer's Dement.* 7, 280–292. doi:10.1016/j.jalz.2011.03.003
- Tang, X., Holland, D., Dale, A.M., Younes, L., Miller, M.I., 2014. Shape abnormalities of subcortical and ventricular structures in mild cognitive impairment and Alzheimer's disease: Detecting, quantifying, and predicting. *Hum. Brain Mapp.* 35, 3701–3725. doi:10.1002/hbm.22431
- Thompson, P.M., Hayashi, K.M., de Zubicaray, G., Janke, A.L., Rose, S.E., Semple, J., Herman, D., Hong, M.S., Dittmer, S.S., Dordrell, D.M., Toga, A.W., 2003. Dynamics of gray matter loss in Alzheimer's disease. *J. Neurosci.* 23, 994–1005. doi:10.1523/JNEUROSCI.2333-03.2003
- Warrington, E.K., James, M., 1991. A new test of object decision: 2D silhouettes featuring a minimal view.

- Cortex 27, 377–383.
- Wechsler, D., 2009. Wechsler Memory Scale-(WMS-IV), New York: The Psychological Corporation.
- Wechsler, D., 1999. Manual for the Wechsler abbreviated intelligence scale (WASI). The Psychological Corporation, San Antonio.
- Wechsler, D., Coalson, D., Raiford, S., 2008. WAIS-IV: Wechsler Adult Intelligence Scale. San Antonio: Pearson, San Antonio.
- Whitwell, J.L., Przybelski, S.A., Weigand, S.D., Knopman, D.S., Boeve, B.F., Petersen, R.C., Jack, C.R., 2007. 3D maps from multiple MRI illustrate changing atrophy patterns as subjects progress from mild cognitive impairment to Alzheimer's disease. *Brain* 130, 1777–1786. doi:10.1093/brain/awm112
- Wisse, L.E.M., Biessels, G.J., Heringa, S.M., Kuijf, H.J., Koek, D.H.L., Luijten, P.R., Geerlings, M.I., 2014. Hippocampal subfield volumes at 7T in early Alzheimer's disease and normal aging. *Neurobiol. Aging* 35, 2039–45. doi:10.1016/j.neurobiolaging.2014.02.021
- Wisse, L.E.M., Gerritsen, L., Zwanenburg, J.J.M., Kuijf, H.J., Luijten, P.R., Biessels, G.J., Geerlings, M.I., 2012. Subfields of the hippocampal formation at 7 T MRI: in vivo volumetric assessment. *Neuroimage* 61, 1043–9. doi:10.1016/j.neuroimage.2012.03.023
- Wolk, D.A., Das, S.R., Mueller, S.G., Weiner, M.W., Yushkevich, P.A., 2016. Medial temporal lobe subregional morphometry using high resolution MRI in Alzheimer's Disease. *Neurobiol. Aging* 1, 1–10. doi:10.1016/j.neurobiolaging.2016.09.011
- Yassa, M.A., 2014. Ground zero in Alzheimer's disease. *Nat. Neurosci.* 17, 146–147. doi:10.1038/nn.3631
- Yassa, M.A., Muftuler, L.T., Stark, C.E.L., 2010a. Ultrahigh-resolution microstructural diffusion tensor imaging reveals perforant path degradation in aged humans in vivo. *Proc. Natl. Acad. Sci. U. S. A.* 107, 12687–12691. doi:10.1073/pnas.1002113107
- Yassa, M.A., Stark, S.M., Bakker, A., Albert, M.S., Gallagher, M., Stark, C.E.L., 2010b. High-resolution structural and functional MRI of hippocampal CA3 and dentate gyrus in patients with amnesic Mild Cognitive Impairment. *Neuroimage* 51, 1242–1252. doi:10.1016/j.neuroimage.2010.03.040
- Yeung, L.-K., Ryan, J.D., Cowell, R.A., Barense, M.D., 2013. Recognition Memory Impairments Caused by False Recognition of Novel Objects. *J. Exp. Psychol. Gen.* doi:10.1037/a0034021
- Yushkevich, P.A., Amaral, R.S.C., Augustinack, J.C., Bender, A.R., Bernstein, J.D., Boccardi, M., Bocchetta, M., Burggren, A.C., Carr, V. a, Chakravarty, M.M., Chételat, G., Daugherty, A.M., Davachi, L., Ding, S.-L., Ekstrom, A., Geerlings, M.I., Hassan, A., Huang, Y., Iglesias, J.E., La Joie, R., Kerchner, G.A., LaRocque, K.F., Libby, L. a, Malykhin, N., Mueller, S.G., Olsen, R.K., Palombo, D.J., Parekh, M.B., Pluta, J.B., Preston, A.R., Pruessner, J.C., Ranganath, C., Raz, N., Schlichting, M.L., Schoemaker, D., Singh, S., Stark, C.E.L., Suthana, N., Tompary, A., Turowski, M.M., Van Leemput, K., Wagner, A.D., Wang, L., Winterburn, J.L., Wisse, L.E.M., Yassa, M. a, Zeineh, M.M., 2015a. Quantitative comparison of 21 protocols for labeling hippocampal subfields and parahippocampal subregions in in vivo MRI: towards a harmonized segmentation protocol. *Neuroimage* 111, 526–41. doi:10.1016/j.neuroimage.2015.01.004
- Yushkevich, P.A., Pluta, J.B., Wang, H., Xie, L., Ding, S.-L., Gertje, E.C., Mancuso, L., Klot, D., Das, S.R., Wolk, D.A., 2015b. Automated volumetry and regional thickness analysis of hippocampal subfields and medial temporal cortical structures in mild cognitive impairment. *Hum. Brain Mapp.* 36, 258–287. doi:10.1002/hbm.22627

- Measured anterolateral entorhinal cortex (alERC), location of earliest AD pathology
- Classified cognitive status with Montreal Cognitive Assessment (MoCA)
- alERC volume was associated with MoCA score in nominally healthy individuals
- First study linking alERC volume with cognitive decline in undiagnosed individuals

ACCEPTED MANUSCRIPT